MAUSAM, **70**, 4 (October 2019), 753-766

551.557.3 (265.2)

Zonally symmetric *vs* asymmetric North Pacific Ocean sea surface temperature influence on Indian summer monsoon through modulation of upper tropospheric circulation

ARINDAM CHAKRABORTY

Centre for Atmospheric and Oceanic Sciences and Divecha Centre for Climate Change

Indian Institute of Science, Bangalore – 560 012, India

e mail : arch@iisc.ac.in

सार - इस अध्ययन में निम्नलिखित प्रश्न उठाए गए हैं: उत्तरी ग्रीष्मकालीन ऋतु में सामान्य परिसंचरण और वायुमंडल की ऊर्ध्वाधर स्थिरता में उत्तरी प्रशांत महासागर (NPAC) के समुद्री सतह के तापमान (SST) के क्षेत्रीय वितरण की क्या भूमिका होती है। परिणामों से पता चलता है कि जब उत्तरी प्रशांत महासागर की क्षेत्रीय सममित समुद्र सतह तापमान उष्णन ऊपरी क्षोभमंडल जेट को उत्तर की ओर शिफ्ट करती है तो क्षेत्रीय एसिमेट्रिक उष्णन और शीतलन पूर्व-पश्चिम दिशा में मध्य अक्षांशीय रॉस्बी तरंगों के चरण को बदल देती है। संचलन में हुए इन परिवर्तनों ने वायुमंडल और वर्षा की ऊर्ध्वाधर स्थैतिक स्थिरता को विशेष रूप से भारतीय क्षेत्र में, संशोधित किया है। विशेष रूप से, जब अल नीनो-दक्षिणी दोलन (ENSO) अनुकूल चरण में नहीं होते हैं, पश्चिमी एनपीएसी (NPAC) में समुद्र सतह के अधिक उष्ण तापमान भारतीय क्षेत्र पर स्थिरता को कम करते हैं, जिससे मानसून की वर्षा बढ़ जाती है। हालांकि, यह घटना भारतीय ग्रीष्मकालीन मानसून में एक ENSO प्रभाव के साथ संयोजन से इसके प्रभाव को बढ़ा सकती है या दबा सकती है। इस परिणाम का उपयोग एक सूचकांक प्राप्त करने के लिए किया जाता है, जो जून-जुलाई में भारतीय ग्रीष्मकालीन मानसून (ISM) वर्षा के 80% से अधिक अंतर को बताता है। चूंकि इस क्षेत्र में जून-सितंबर तक की कुल वर्षा में जून-जुलाई लगभग 50% का योगदान देता है, इस शोध से भारतीय ग्रीष्मकालीन मानसून (ISM) का संभावित पूर्वानुमान बढ़ जाता है। अंत में, युग्मित मॉडल इंटरकम्पेरिसन प्रोजेक्ट (सीएमआईपी 5) से ऐतिहासिक सिमुलेशन का उपयोग करते हुए, हम बताते हैं कि उत्तरी प्रशांत महासागर पर समुद्र सतह तापमान विसंगतियां एन्सो (ENSO) और भारतीय ग्रीष्मकालीन मानसून के बीच संबंधों की मजबूती को प्रभावित करती हैं। इस अध्ययन में प्रस्तावित तंत्र का उपयोग सामान्य परिसंचरण मॉडल के कौशल का निदान करने के लिए किया जा सकता है। ऊपरी ट्रोपोस्फेरिक परिसंचरण के मॉड्यूलेशन के माध्यम से भारतीय गर्मियों में मानसून पर असममित उत्तरी प्रशांत महासागर की समुद्री सतह के तापमान के अनुपात में सममित समरूपता होती है।

ABSTRACT. This study asks the following question: what role the zonal distribution of sea surface temperature (SST) of North Pacific Ocean (NPAC) plays in the general circulation and vertical stability of the atmosphere during boreal summer season. Results here show that while zonally symmetric SST warming of NPAC shifts the upper tropospheric jet northward, zonally asymmetric warming and cooling alter the phase of mid latitude Rossby waves in east-west direction. These changes in circulation modify the vertical static stability of the atmosphere and precipitation, particularly in the Indian region. In particular, warmer SSTs in the western NPAC reduce the stability over Indian region leading to an enhanced monsoon precipitation even when El Nino-Southern Oscillation (ENSO) is not in favorable phase. In conjunction with an ENSO forcing, however, this phenomenon can augment or suppress its impact on Indian summer monsoon. This result is used to derive an index that explains more than 80% of the interannual variance of Indian summer monsoon (ISM) precipitation in June-July. Since June-July contributes about 50% to the total June–September precipitation in this region, this discovery increases the potential predictability of ISM. Finally, using historical simulations from the Coupled Model Intercomparison Project (CMIP5), we show that SST anomalies over NPAC strongly influence the strength of the relationship between ENSO and Indian summer monsoon. The mechanism proposed in this study can be used to diagnose the skill of general circulation models.

Key words – North Pacific Ocean SST, Rossby waves, Subtropical jet, Atmospheric stability, Indian summer monsoon, CMIP5 models.

1. Introduction

The El Nino-Southern Oscillation (ENSO) modulates climate around the globe including circulation (Seager *et al.*, 2003; Lu *et al*., 2008) and convection - As seen in observations (Sikka, 1980; Srivastava *et al*.. 2019) and numerical model simulations (Lau and Nath, 2000) and potential prediction (Chattopadhyay and Bhatla, 1993). During an El Nino in boreal summer, upper tropospheric anomalous divergent winds over the

equatorial Pacific Ocean induce convergence over south Asia. This modulation of the Walker circulation results in descent over south Asia and reduction in ISM rainfall (ISMR). However, there were several exceptions to this general finding in the past century when reliable datasets of precipitation and SST were available. Nino 3.4 SST explains about 34% of the interannual variations of ISMR and the strength of this relationship varies in multi-decadal time scales (Kumar *et al*., 1999; Torrence and Webster, 1999; Krishnamurthy and Goswami, 2000; Meehl and Arblaster, 2011; Hunt, 2014; Srivastava *et al*., 2019). It is possible that such linkage between equatorial Pacific SST and ISMR be influenced by quasi-biennial oscillation (Chattopadhyay and Bhatla, 2002; Bhatla *et al*., 2013).

Apart from its simultaneous impact, the delayed impact of ENSO is also important especially during summer ENSO neutral years when dominant forcing is absent (Chakraborty, 2018). It has been shown that decaying or growing ENSO has different impacts on east Asian summer monsoon (Ronghui and Yifang, 1989; Shen and Lau, 1995; Chang *et al*., 2000, Wang *et al*., 2000). A relationship between changing nature of the sea level pressure at Darwin and rainfall of ISM was shown by Shukla and Paolino (1983) and Shukla and Mooley (1987). However, these impacts are not symmetric for decaying and developing ENSO. Chakraborty (2018) have shown that La Nina of previous winter decreases ISMR even during ENSO neutral summer. This impact is severe and causes drought during El Nino summer. Such delayed impact of ENSO on ISMR is due to zonal propagation of surface pressure anomaly with change in SST of the equatorial Pacific Ocean. For a transition from winter La Nina, positive pressure anomalies appear over western central Asia during boreal summer decreasing the incoming moisture flux to Indian subcontinent (Chakraborty and Agrawal, 2017).

The west and the north Pacific Ocean impact ISM from intraseasonal to interdecadal time scales. Westward propagating oscillatory modes with time period 10-20 days from west Pacific Ocean can initiate break phase of ISM (Krishnamurti and Ardanuy, 1980; Chen and Chen, 1993). The intensity of this 10-20 day oscillations is related to SST of west Pacific warm pool through Gill-type circulation response (Baohua and Ronghui, 2002). Constructive and destructive overlapping of the phases of this westward propagating 10-20-day high frequency intraseasonal variation (HF-ISO) and northward propagating 30-60-day low-frequency intraseasonal variation (LF-ISO) give rise to active and break spells of rainfall over central India (Karmakar *et al*., 2017).

The decadal climate variability of the NPAC, the Pacific Decadal Oscillation (PDO) (Zang *et al*., 1997; Mantua *et al*., 1997) impacts ISM in interdecadal time scales (Krishnan and Sugi, 2003). While ENSO and PDO could be somewhat related at interdecadal time scales (Nidheesh *et al*., 2017), different combinations of phases of ENSO and PDO having different impacts on ISM (Krishnamurthy and Krishnamurthy, 2014). This study hypothesized, based on mechanism proposed by Vimont *et al*. (2001, 2003) that the SST and surface pressure anomalies of NPAC in the preceding winter impact the summer SST and trade winds along the Equator, which modify the Hadley and the Walker circulations. Modulation of circulation through this *seasonal footprinting* affects the ISM. As a result, SST of north Pacific Ocean in the previous winter can be a precursor to the intensity of summer monsoon over Indian region (Peings *et al*., 2009). The combined effects of ENSO and PDO on the spatial distribution of droughts in northern winter is illustrated by (Wang *et al*., 2014). Warming of western parts of subtropical oceans during northern winter can impact air temperature over the neighboring continents through modulation of circulation (Kaspi and Schneider, 2011).

During phases of canonical ENSO, a large region over equatorial Pacific Ocean (from the dateline to far eastern parts) becomes warmer or colder. The zonally asymmetric flavor of ENSO, the ENSO Modoki, shows different impacts on climate around the globe when compared to a conventional ENSO (Ashok *et al*., 2007). However, a comprehensive study of the impact of different spatial distributions of SST away from the Equator during northern summer season on the general circulation and convection of the atmosphere has not been reported so far. In particular, a detailed mechanism relating SST over North Pacific Ocean to Indian summer monsoon remains elusive to date. This study investigates the role of zonal symmetry *vs* asymmetry in SST of NPAC in atmospheric circulation and ISM precipitation.

2. Data sets and methodology

The SST data used is the National Oceanic and Atmospheric Administration (NOAA) Optimum Interpolated (OI) Version 2, global gridded monthly mean product (Reynolds *et al*., 2002). This data set is available from November 1981 through present. Monthly mean and all-India homogeneous regions averaged rainfall data set (Mooley and Parthasarathy, 1984), from 1871 through 2012, is used to study interannual variations. This study also uses rain gauge based, gridded (1 × 1 degree) daily data (Rajeevan *et al*., 2006) to study spatial variability. The PDO index (PDOI) was obtained from http://jisao.washington.edu/pdo/PDO.latest (Zang *et al*., 1997; Mantua and Hare, 2002).

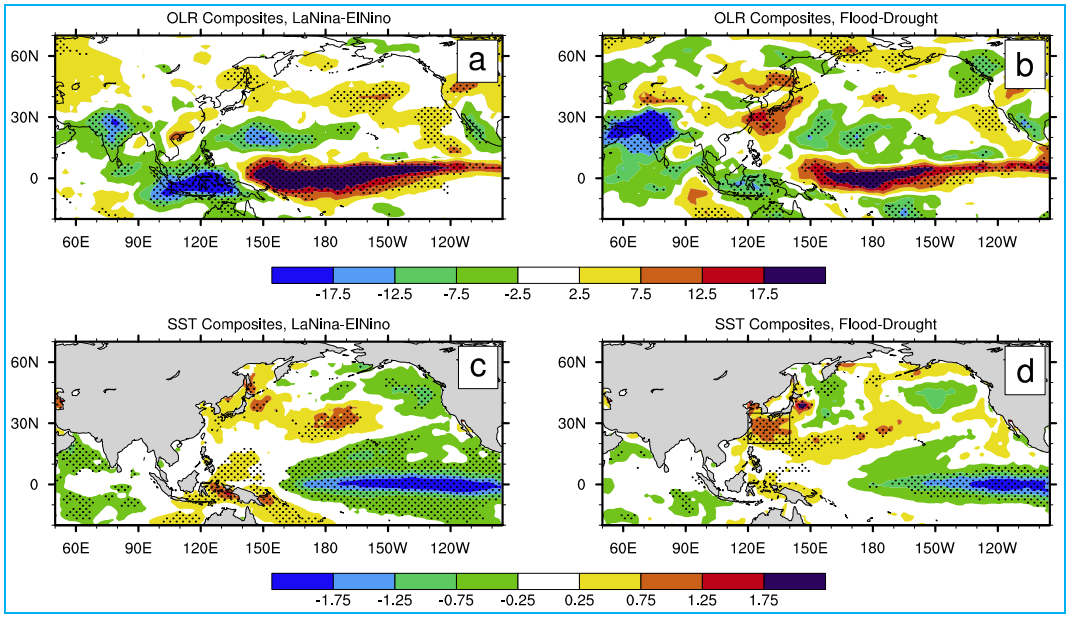

Figs. 1(a-d). Composites of June-July mean outgoing longwave radiation (OLR) for (a) *LaNina−ElNino* years; and (b) *flood - drought* years. (c) and (d): same as (a) and (b), but for SST. The dotted regions indicate significance at 90% level calculated using a student's *t*-test

Temperature, specific humidity and horizontal wind components of the atmosphere were obtained from European Centre for Medium-Range Weather Forecasts (ECMWF) Interim Reanalysis (Dee *et al*., 2011). The outgoing longwave radiation (OLR) data used here was spatially interpolated and daily averaged, derived from multiple satellite measurements (Liebmann, 1996). In order to use satellite derived SST and ground-based observed precipitation, this study uses the common period of these data sets, *viz*., 1982 through 2012.

Anomalies for all data sets were calculated by removing the monthly climatology. The global mean linear trend in SST was removed at each grid point to eliminate signatures of global warming. In order to obtain a time series, the detrended SST anomalies were averaged over a region & normalized. All composites were calculated based on these monthly-standardized SST time series.

3. Results

3.1. *Zonal symmetry of SST of North Pacific Ocean and Indian summer monsoon*

Composites of June-July mean OLR anomaly for the La Nina (Nino 3.4 SST or N34SST < -0.5) *minus* El Nino (N34SST > +0.5) years [Fig. 1(a)] show large region of reduced convection over the entire equatorial Pacific Ocean, accompanied by enhanced convection over maritime continents as well as the Indian region. This signifies the typical modulation of Walker circulation during ENSO phases. Fig. 1(b) shows similar OLR composites for flood (precipitation > +1) *minus* drought (precipitation < -1) years of ISM. Note that, the decrease in OLR in central and north India are stronger for *flood-drought* years as compared to *LaNina-ElNino* years. This result is consistent with the way these composites were defined, given the fact that intensities of N34SST and ISM precipitation do not have a one-to-one relationship.

Note also that, during *flood-drought* years of ISM, OLR over western NPAC is anomalously high (>10 W m^{-2}). A region of reduced OLR in the north-central Pacific Ocean accompanies this aforementioned positive OLR anomaly. Such east-west dipole in OLR for *LaNina-ElNino* years is absent [Fig. 1(a)].

Composites of June-July mean SST anomaly for *flood-drought* years show a region of warming, of about 1 ^{o}C, in western NPAC [Fig. 1(d)]. This is accompanied by cooling of central NPAC, consistent with the differences in OLR [Fig. 1(b)]. The SST differences between ENSO phases [Fig. 1(c)] show an east-west spatial coherence in the NPAC. These results are also evident in the latitudinal mean of the composites, shown in Figs. 2(a&b). It is evident that a large region over western NPAC carries a spatially coherent signature of east-west dipole of SST as seen in the composites [Fig. 1(d)]. We have chosen the region 120-140° E, 20-35° N (will be termed as NP1) to represent SST variability in the western NPAC. The standardized SST anomaly of NP1 will be termed as NP1SST in this paper.

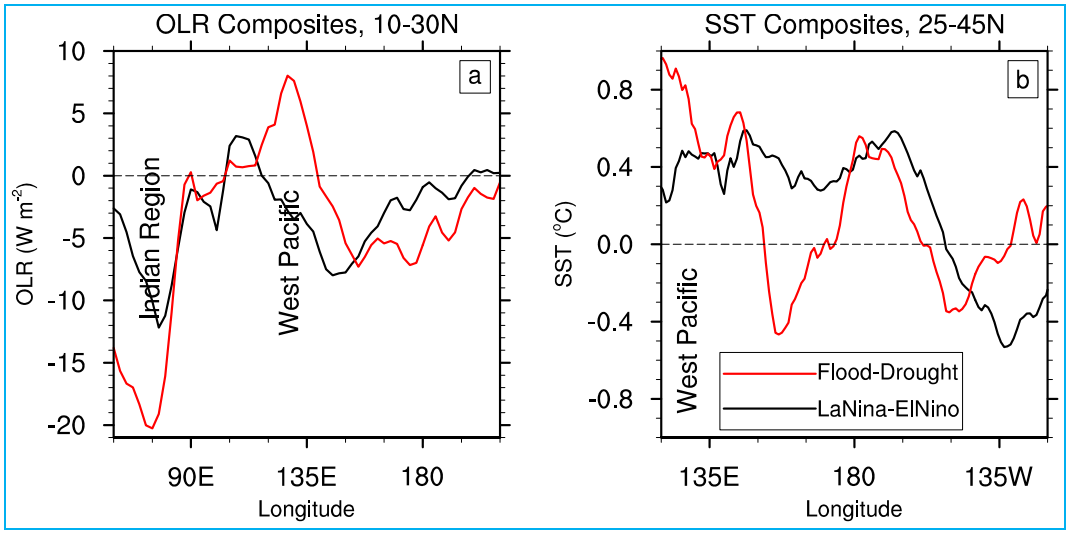

Figs. 2(a&b). Composites of June-July mean OLR (W/m^2) and SST (°C) anomalies for LaNina - ElNino years (black) and flood - drought years of Indian summer monsoon precipitation (red). (a) The OLR is averaged over Indian latitudes (10-30° N) and (b) SST is averaged over north Pacific Ocean (25-45° N)

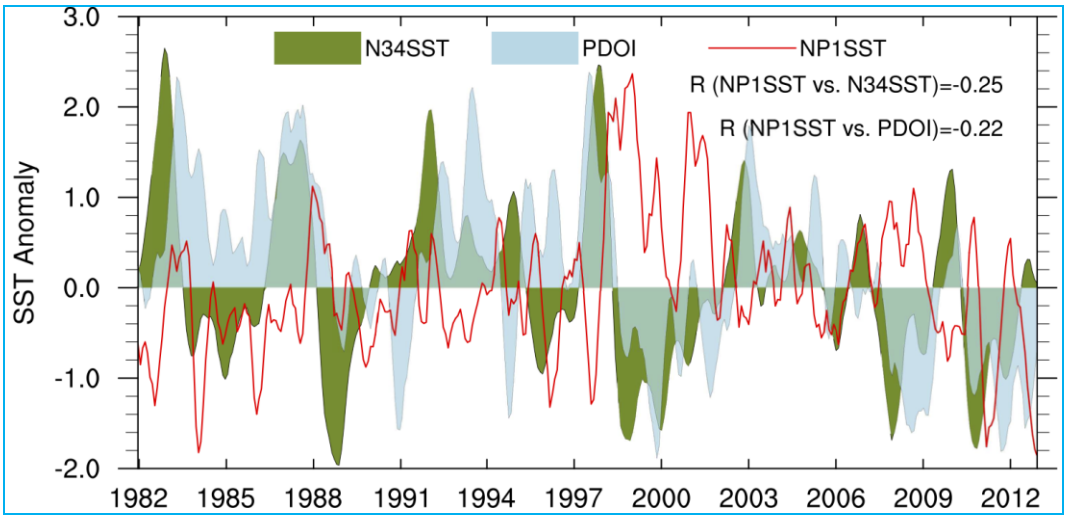

Fig. 3. The time series of monthly mean SST over Nino 3.4 (N34SST) and that over north-west Pacific Ocean (120-140° E, 20-35° N; NP1SST), along with the time series of Pacific Decadal Oscillation Index (PDOI). The time series were standardized by their respective standard deviations and 5-month running mean was performed before plotting to remove high-frequency variations. The linear correlation coefficients (R) between NP1SST, N34SST and PDOI are indicated inside the panel

NP1SST is poorly correlated with N34SST (R = -0.25) and PDOI (R = -0.22) (Fig. 3). It can be noticed that there are several events of strong positive (>+1; *P*) and strong negative (<-1; *N*) NP1SST without a favorable phase of ENSO or PDO. By a favorable phase with respect to ENSO (PDO) we mean opposite anomalies of NP1SST and N34SST (PDOI). This comes from the fact that the signature of ENSO and PDO is present over north-western Pacific Ocean with an anomaly opposite to that over Nino 3.4 (PDOI). Fig. 4 shows that about 50% of the *P* NP1SST occurred in negative phase of ENSO (N34SST <-0.5) and cool phase of PDO (PDOI <-1.0). Similarly, about 50% of the *N* NP1SST occurred in positive phase of ENSO (N34SST > +0.5) and warm phase of PDO (PDOI>+1.0).

3.2. *Changes in circulation and convection*

We categorize the northern hemisphere early summer monsoon months (June and July) when NP1SST is strongly positive or negative with a favorable phase of ENSO or PDO (call it the symmetric mode) and when NP1SST is strongly positive or negative without a favorable phase of ENSO and PDO (call it the asymmetric

mode). The justification for the prefixes symmetric or asymmetric will be evident from the associated spatial distribution of SST anomalies, discussed below:

The SST composites in northern summer months for *P-N* asymmetric mode [Fig. 5(a)] show signature of east-west asymmetry in anomaly over NPAC. Note also that the signs of SST anomaly of western NPAC and eastern equatorial Pacific Ocean could be same in an asymmetric mode. The SST composites for *P-N* symmetric mode [Fig. 5(b)] show zonally coherent warming and cooling of the north and equatorial Pacific Ocean, respectively. This spatial mode of the NPAC SST can be contrasted with that of *N-P* N34SST [Fig. 5(c)] which shows zonally symmetric cooling in the equatorial Pacific Ocean and weaker warming in the north. We would like to clarify here that, some of the months identified as *P* or *N* N34SST may also be included in the *P* or *N* symmetric or asymmetric modes. These composites, signifying patterns associated with Nino 3.4 SST variations, were deliberately constructed to compare with the other two modes defined in this study.

The asymmetric mode leads to zonally incoherent changes in upper tropospheric (200 hPa) geopotential height [Fig. 5(d)]. This is unlike the changes for *P-N* symmetric mode [Fig. 5(e)] when a zonally coherent increase in geopotential is noticed over this region. The changes in geopotential height over NPAC were smaller and not significant for *N-P* N34SST [Fig. 5(f)].

The changes in geopotential height of 200 hPa lead to changes in zonal and meridional winds [Figs. 6(a-f)] through geostrophic balance at higher latitudes. East-west asymmetric anomalous geopotential [Fig. 6(d)] leads to east-west asymmetric alteration of midlatitude zonal wind [Fig. 6(a)]. On the other hand, Fig. 6b suggests a near circumglobal northward shift of the subtropical jet stream for *P-N* symmetric mode. The northward shift of the axis of the jet over central NPAC (Indian region) is as much as 20 (15) degrees [Figs. 7(a-c)]. This can have significant impact on the wave propagation and subsequent teleconnection between Pacific Ocean SST and ISM (Shaman & Tziperman, 2007). Changes in zonal wind for *N-P* N34SST months are primarily confined to the tropics [Fig. 6(c)].

The east-west variation in SST for *P-N* asymmetric mode leads to a strong change in meridional winds at 200 hPa [Fig. 6(d)]. This indicates a phase shift of upper tropospheric Rossby waves, that can induce anomalous divergence and convergence associated with ascent and descent along its path (Ding and Wang, 2005 & 2007). In particular, it supports upper level divergence over Indian region for *P-N* asymmetric mode. No strong changes in midlatitude Rossby waves are noticed with zonally

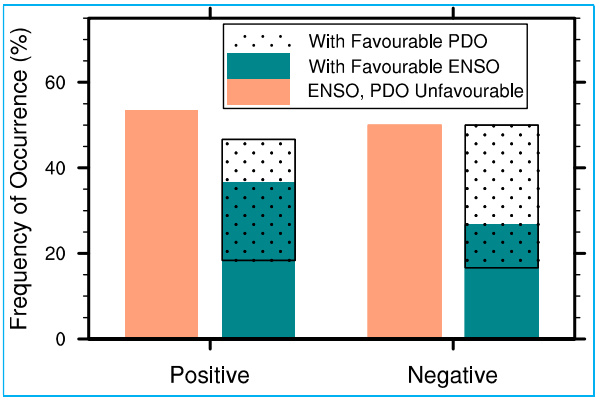

Fig. 4. Per cent of occurrences, in the monthly mean data sets of NOAA OI SST-v2 during 1982 to 2012, of positive or negative NP1SST associated with N34SST and PDOI

symmetric SST anomaly in NPAC [Fig. 6(e)] or during ENSO phases [Fig. 6(f)]. Therefore, it can be concluded that while zonally symmetric off-equatorial SST anomalies impact the midlatitude jet stream, zonally asymmetric off-equatorial forcing modulate phase of the Rossby waves. This figure also suggests that the SSTs of NPAC can impact zonal and meridional winds at other longitudes in the Indo-Pacific region, possibly through advection of geopotential (Hoskins and Ambrizzi, 1993; Ambrizzi and Hoskins, 1997).

Figs. 8(a-f) shows the corresponding changes in vertical moist-static stability of the atmosphere (VMS). Moist static energy (M) of a volume of the atmosphere per unit mass is defined as:

$$M = C_p T + gz + Lq \quad (1)$$

where, T, q and z are temperature, specific humidity and geopotential height of the volume considered, respectively; C_p, g and L are heat capacity at constant pressure for moist air, acceleration due to gravity and latent heat of evaporation of water, respectively. MSE of an atmospheric column is a measure of net amount of energy. A higher value of MSE near the surface, for example, would indicate high temperature and/or moisture that can lead to increase in convective available potential energy (CAPE) and enhanced convection (Neelin and Held, 1987; Srinivasan and Smith, 1996; Nanjundiah and Srinivasan, 1999; Chakraborty *et al*., 2006, 2014). Accordingly, vertical moist-static stability (VMS) is defined as the difference in mass weighted MSE between the top and bottom layers of the atmosphere:

$$VMS = \frac{1}{p_t - p_m}\int_{p_m}^{p_t} M\,dp - \frac{1}{p_m - p_b}\int_{p_b}^{p_m} M\,dp \quad (2)$$

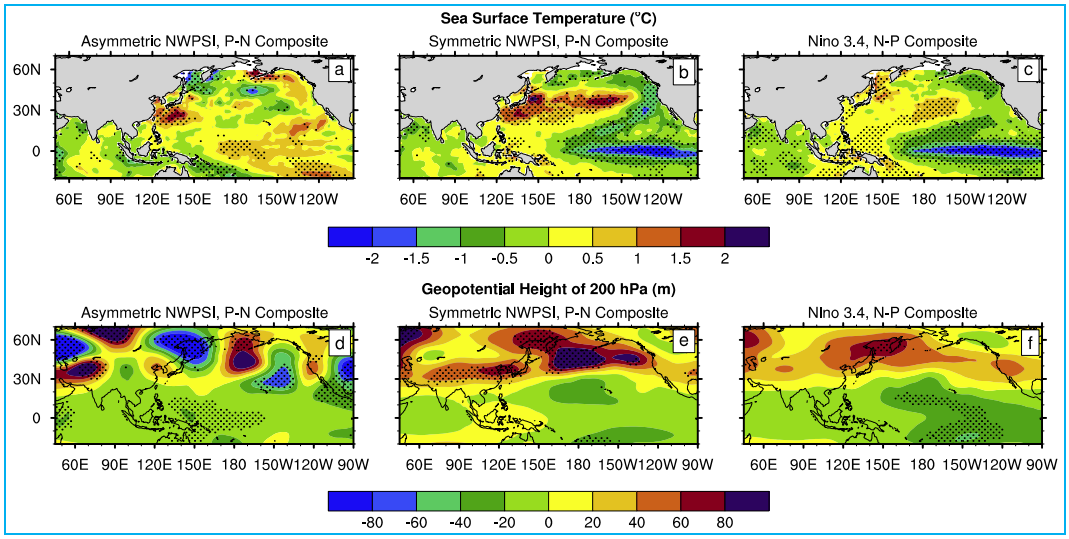

Figs. 5(a-f). Anomalies of SST (in ◦C) and geopotential height of 200 hPa (in m) for different SST conditions in Pacific Ocean. Top and bottom panels show the changes in SST and 200 hPa geopotential height, respectively. Left, middle and right panels show *P-N* composites for asymmetric mode, *P-N* composites for symmetric mode and *N-P* composites for N34SST, respectively. The dotted regions indicate significance at 90% level calculated using a student's *t*-test

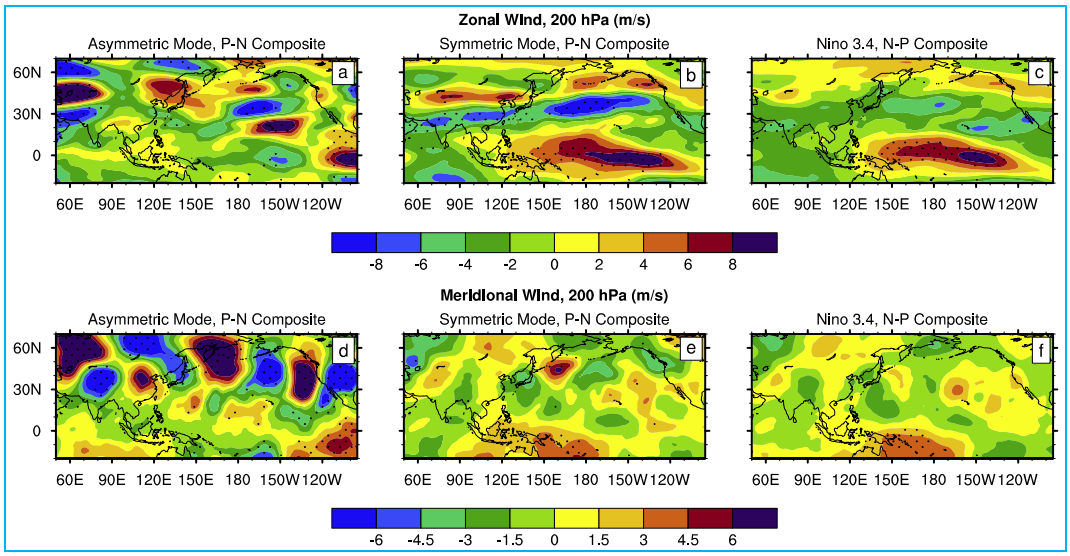

Figs. 6(a-f). Same as in Figs. 5(a-f) but for zonal and meridional winds

where, p_b, p_m and p_t are bottom, middle and top pressure levels of the column; taken as the surface pressure, 400 hPa and 100 hPa, respectively. A decrease (an increase) in VMS can lead to enhanced (reduced) convection at that column. During *P-N* asymmetric mode [Fig. 8(a)], changes in VMS over northern hemisphere follow a wave train pattern much similar to the Rossby wave phase shift [Fig. 6(d)]. In particular, VMS over Indian region is reduced indicating favored convection.

A large region from central NPAC to the Indian subcontinent experiences decrease in VMS when NPAC is warmer in a zonally coherent manner [Fig. 8(b)], that follows the pattern of changes in zonal wind at 200 hPa [Fig. 6(b)]. Spatial pattern of changes in VMS for *N-P* N34SST [Fig. 8(c)] is similar to that for the *P-N* symmetric mode, albeit with reduced magnitudes in the northern hemisphere. Notice that the differences in VMS along equatorial Pacific Ocean for the symmetric mode and N34SST composites are large, indicating influence of ENSO. However, such differences for the asymmetric mode are small and not statistically significant. In fact, differences over maritime continents are opposite in sign for *P-N* asymmetric mode to *P-N* symmetric mode. This

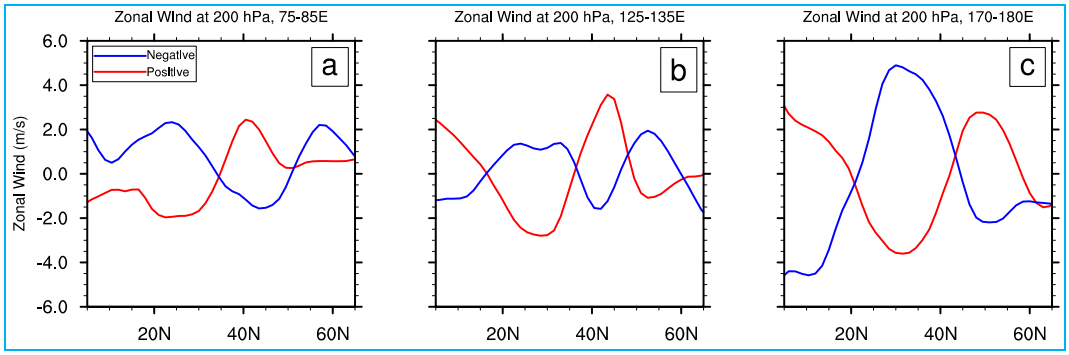

Figs. 7(a-c). Composite anomaly of zonal wind at 200 hPa for positive (P) and negative (N) symmetric mode of NPAC, averaged over (a) 75-80° E; (b) 125-135° E; and (c) 170-180° E

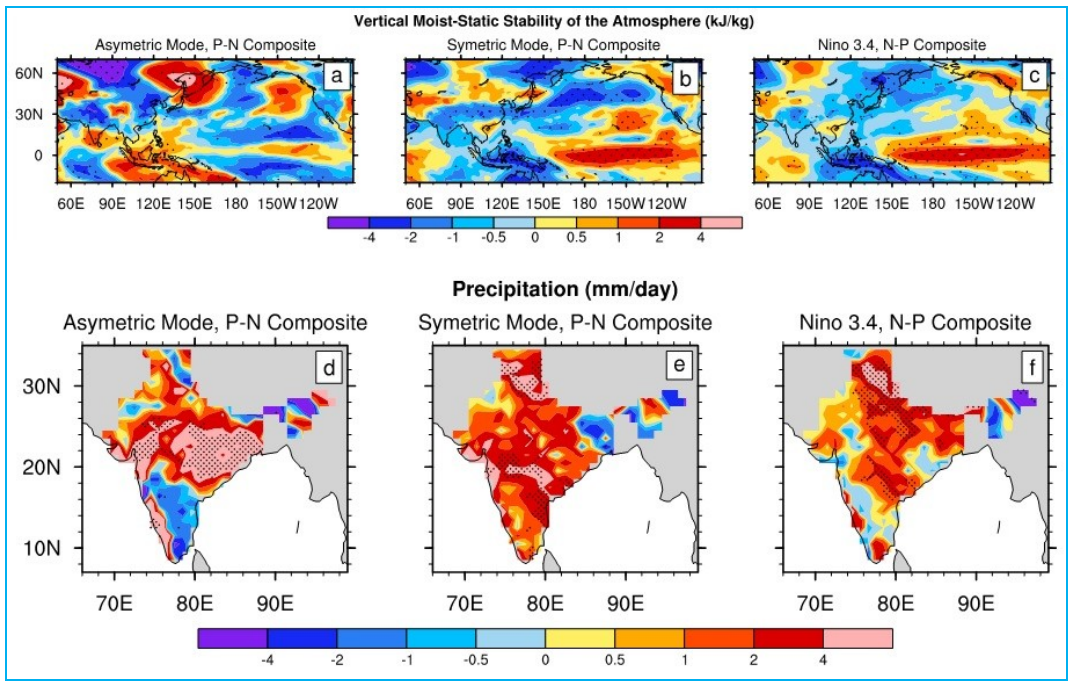

Figs. 8(a-f). Same as in Figs. 5(a-f) but for vertical moist static stability (VMS) and precipitation

indicates that changes in VMS in northern hemisphere in the asymmetric mode are independent of the ENSO related SST changes along the equator.

The *P-N* asymmetric mode composites show strong increase in precipitation in central India [Fig. 8(d)], associated with decrease in south Indian peninsula and northeast India. These are consistent with changes in Rossby wave phase [Fig. 6(d)] and decrease in VMS [Fig. 8(a)]. The *P-N* symmetric mode precipitation composites show more spatially coherent differences in the Indian region [Fig. 8(e)]. These are possibly signatures of in-phase impact of ENSO and PDO. ENSO related precipitation changes are also spatially coherent over the entire Indian region. Moreover, ENSO strongly impacts precipitation in the foothills of the Himalayas [Fig. 8(f)], consistent with the changes in VMS [Fig. 8(c)].

3.3. *The Indo-Pacific SST Index*

Can SST of NPAC be used to explain the interannual variability of ISM? We answer this question evaluating the combined effect of NP1SST and SST of three other key regions of the global oceans known to have impact on ISM. These three regions are: Nino 3.4, the eastern Equatorial Indian Ocean (EEIO; 80-110° E, 10° S-Equator) and the central NPAC (NP2; 155-175° E, 30-45° N). The definition of EEIO here is close to that of (Saji *et al*., 1999). Interannual variation of June-July mean SST of NP2 is highly correlated with the PDOI (R = -0.77)

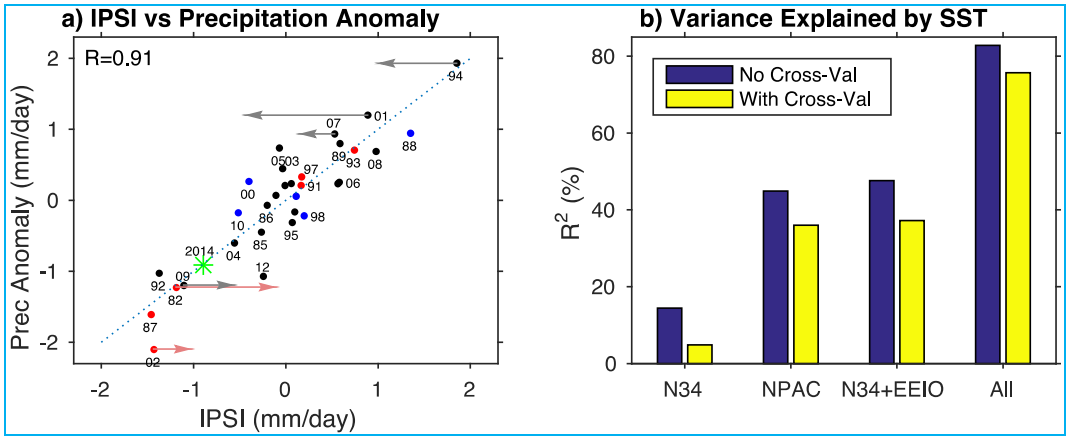

Figs. 9(a&b). (a) Scatter plot between Indo-Pacific SST Index (IPSI) and precipitation over India in June-July. Few important years are indicated by their last two digits. Years when N34SST was $^{[1]}_{SEP}$ > 0.5, < −0.5 and between -0.5 and 0.5 are indicated in red, blue and black colors, respectively. Arrows indicate the IPSI values constructed without including NP1 and NP2 during few extreme $^{[1]}_{SEP}$ years. (b) Interannual variation of precipitation explained by SST (R^2) for different combinations of regions with and without cross-validation

and thus SST of this region is representative of PDO. A multiple linear regression (MLR) between June-July mean SST of these four domains and precipitation in India is constructed. The combined index is termed as the Indo-Pacific SST Index (IPSI) and is defined as

$$IPSI = c_1 T_{NP1} + c_2 T_{NP2} + c_3 T_{n34} + c_4 T_{EEIO} \qquad (3)$$

where, T_{NP1}, T_{NP2}, T_{N34} and T_{EEIO} are SST anomalies of NP1, NP2, Nino 3.4 and EEIO, respectively; c_1, c_2, c_3 and c_4 are coefficients obtained from the MLR and carry the units mm day^{-1}/(°C). The units of IPSI are mm day^{-1}. The values of c_1, c_2, c_3 and c_4 are 1.43, -0.70, -0.31 and -2.19, respectively, determined using a multilinear regression between the predictand (IPSI) and the predictands (T_{NP1}, T_{NP2}, T_{N34} and T_{EEIO}).

A scatter plot between IPSI and observed precipitation anomaly in India during June-July from 1982 through 2012 is shown in Fig. 9(a). IPSI well captures the observed precipitation anomaly in most of the years. The linear correlation coefficient between these two quantities is 0.91. Therefore, IPSI can explain about 82% of the interannual variance of June-July mean precipitation in the satellite era. The precipitation anomaly (IPSI) of June-July 2014, estimated using regression coefficients obtained from 1982-2012 data sets and then applied to the observed SST anomaly of 2014, is indicated by a green star on Fig. 9(a). Note that this estimation well captures the observed deficient precipitation in this year.

IPSI values were also calculated without using SST of NP1 and NP2. Arrows in Fig. 9(a) indicate these values during few extreme years. This suggests that SST of NPAC is necessary to adequately explain the extreme positive (1994, 2001, 2007) and negative (1982, 2002, 2009) monsoon precipitation in India in June-July.

To show further that SST of NPAC plays an important role in determining interannual variation of precipitation in India, we have calculated the variability (R^2) explained by SST for different combinations of regions [Fig. 9(b)], using MLR, as discussed above. In addition to the regular regression results shown above (without cross-validation), the MLR was also performed with cross-validation (where the year in concern was not used to calculate the regression coefficients). This way, the impact of the particular years does not influence the value of the coefficients. These coefficients are then applied to SST anomaly of the year concerned to calculate IPSI (the rainfall anomaly). This procedure is repeated for all the 31 years (1982-2012). In order to calculate the index for different combinations of regions (regressors), MLR was calculated separately for every combination, instead of using the coefficients values mentioned above. For example, when we used NP1 and NP2 to predict IPSI, a new set of regression coefficients were derived instead of using those of Eqn 3 (c1 and c2). This way, NP1 and NP2 together will explain maximum variance possible in IPSI. This is different than taking c1 and c2 (of Eqn 1) since there is non-zero cross correlation between NP1 and NP2 SST. Fig. 9(b) shows that when SST of NP1 and NP2 are used, in conjunction with that of Nino 3.4 and EEIO, the interannual variability explained is highest. Moreover, the differences between variance explained with cross-validation and without cross-validation are smaller when more regions are included for regression.

TABLE 1

The list of CMIP5 models along with their horizontal resolution (of the atmospheric component, in number of latitude × longitude) used in this study

S. No.	Model Name	Resolution
1.	bcc-csm1-1	64 × 128
2.	bcc-csm1-1-m	160 × 320
3.	CCSM4	192 × 288
4.	CESM1-CAM5	192 × 288
5.	CMCC-CESM	48 × 96
6.	CMCC-CM	240 × 480
7.	CMCC-CMS	96 × 192
8.	CNRM-CM5	128 × 256
9.	CNRM-CM5-2	128 × 256
10.	CSIRO-Mk3-6-0	96 × 192
11.	FIO-ESM	64 × 128
12.	GFDL-CM2p1	90 × 144
13.	GFDL-CM3	90 × 144
14.	GFDL-ESM2G	90 × 144
15.	GFDL-ESM2M	90 × 144
16.	GISS-E2-H	90 × 144
17.	GISS-E2-H-CC	90 × 144
18.	GISS-E2-R	90 × 144
19.	GISS-E2-R-CC	90 × 144
20.	HadCM3	73 × 96
21.	HadGEM2-AO	145 × 192
22.	HadGEM2-ES	145 × 192
23.	inmcm4	120 × 180
24.	IPSL-CM5A-LR	96 × 96
25.	IPSL-CM5A-MR	143 × 144
26.	IPSL-CM5B-LR	96 × 96
27.	MIROC5	128 × 256
28.	MIROC-ESM	64 × 128
29.	MIROC-ESM-CHEM	64 × 128
30.	MPI-ESM-LR	96 × 192
31.	MPI-ESM-MR	96 × 192
32.	MPI-ESM-P	96 × 192
33.	MRI-CGCM3	160 × 320
34.	MRI-ESM1	96 × 144
35.	NorESM1-M	96 × 144
36.	NorESM1-ME	96 × 144

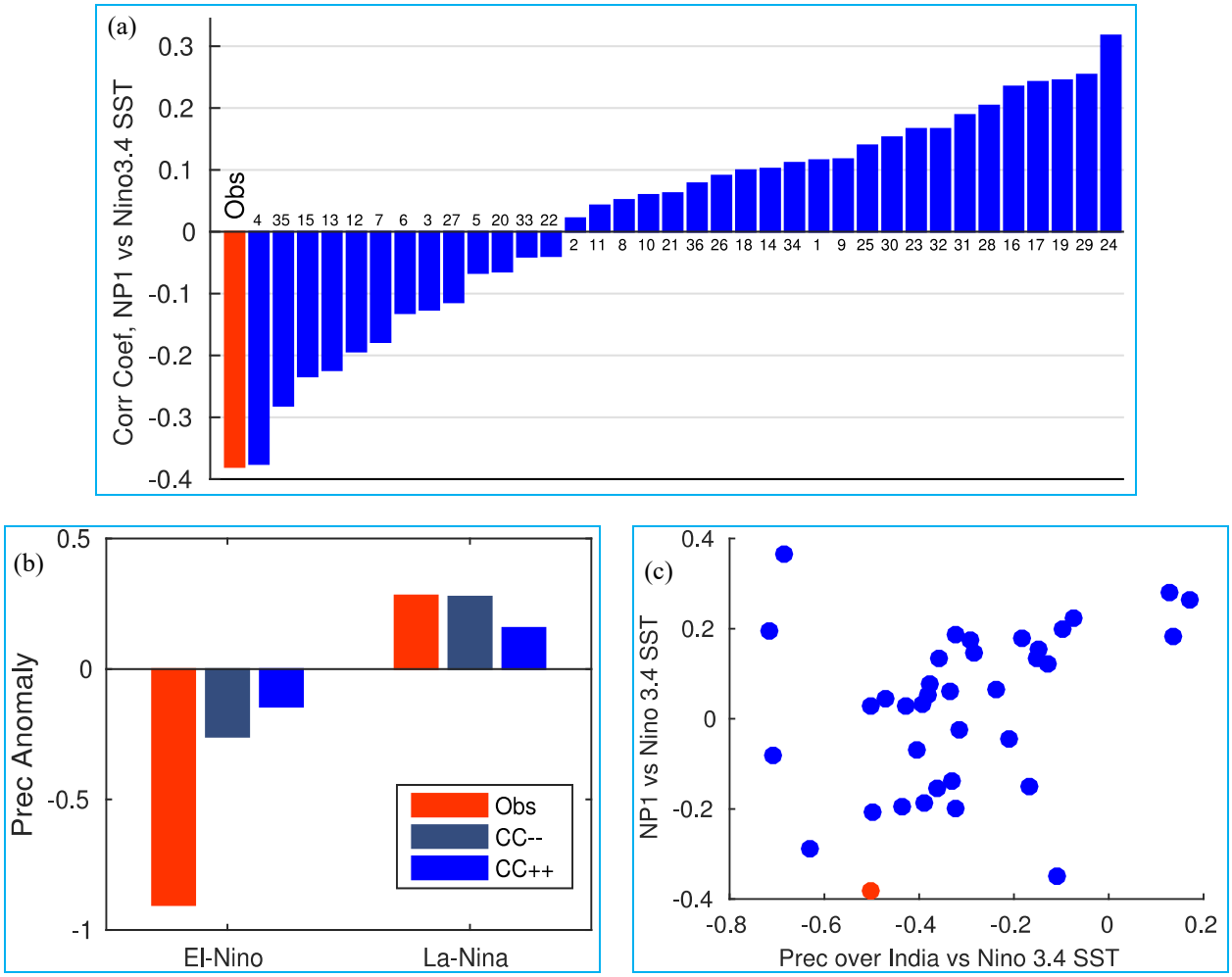

Figs. 10(a-c). (a) Observed (red bar) and 36 CMIP5 model simulated interannual correlation between SST anomalies over Nino 3.4 and NP1, in June-September. The model numbers correspond to Table 1. (b) Composite of standardized (by the respective climatology) rainfall anomaly over Indian region (70-90° E, 5-25° N) in June-September from observations (GPCP) and 6 (10) CMIP5 models with highest negative (positive) correlation between Nino 3.4 and NP1 SST anomalies. (c) Scatter plot of interannual correlation between Nino 3.4 and NP1 SST *vs* Nino 3.4 SST and rainfall over Indian region in June-September. The observed value is shown in red color

This relationship is relatively poor for the later months of Indian summer monsoon (August-September; R = 0.48). We guess that this could be related to climatological position of the subtropical jet in August-September when it shifts northward compared to June-July. Since the Rossby waves are south of this jet, the impact of NWPSI decreases when they are further north of the Indian region. It also could be related to the internal dynamics of the atmosphere-ocean system that feeds back to itself after the monsoon is set up over south Asia (Chakraborty *et al*., 2006). This possibly suggests that different factors, including SST pattern, play role in determining ISM precipitation during its early and late phases and therefore, need to be studied separately (Terray *et al*., 2003; Chakraborty *et al*., 2006; Boschat *et al*., 2010). However, our study shows that SST over four regions can explain 82% of the interannual variability monsoon rainfall over India during the first half of the season (June-July), the phase most important for agriculture over the country.

3.4. *Do CMIP5 models capture the observed relationship between SST of north Pacific Ocean and Indian Summer Monsoon?*

Finally, we show here evidence from CMIP5 model ensembles that a correct simulation of SST over north west Pacific Ocean during ENSO events is important for the realistic simulation of Indian summer monsoon during El Nino and La Nina. For this, we take advance of the fact that observed correlation between SST anomalies over Nino 3.4 and NP1 is -0.39 [June-September mean SST of

1982-2012 from (Reynolds *et al.*, 2002)]. We categorize 36 CMIP5 models (list of models in Table 1) according to their simulated correlation between SST anomalies over Nino 3.4 and NP1 in June-September in the historical simulation period [1861-2005; Fig. 10(a)], along with corresponding observation value. Many CMIP5 models do not show a realistic seasonal cycle or rainfall over Indian region (Jayasankar *et al*., 2015). Thus, averaging over four months (June-September) is more likely to capture the boreal summer season simulated by these models. However, the results presented are qualitatively similar when only June-July months are considered (not shown). From Fig. 10(a) we note that CMIP5 model simulated correlations vary in a wide range (-0.38 to 0.32), with 13 models having –ve (as in observations) and 23 models having +ve correlation.

Next, we chose 6 (10) models with highest negative (positive) correlation [from Fig 10(a)]. A composite of rainfall anomaly over Indian region (70-90° E, 5-25° N) among these models during El Nino and La Nina years, along with the corresponding observed values are shown in Fig. 10(b). We define El Nino (La Nina) of the model when June-September mean SST anomaly over Nino 3.4 is above +0.5 K (below -0.5 K). Clearly, models those capture the correct relationship in SST between Nino 3.4 and NP1 (-ve correlation, denoted by CC--) outperform the models of the other category (+ve correlation, denoted by CC++) in capturing the intensity of anomaly in rainfall over Indian region, both during El Nino and La Nina years.

We further extend these results to understand how SST over NP1 impacts the strength of ENSO-Indian summer monsoon relationship in these CMIP5 models. In Fig. 10(c) we show scatter plots of the interannual correlation between SST anomaly over Nino 3.4 and rainfall over Indian region, *vs*. interannual correlation between SST anomalies over Nino 3.4 and NP1. Note that, the CMIP5 models show wide range of ENSO-monsoon relationships (measured by the linear correlation coefficient), from about -0.7 to 0.2, while the observed relationship is about -0.5 (marked in red color). Such wide range in the ENSO-monsoon relationship in CMIP5 models was noted in simultaneous (Sperber *et al*., 2013) as well as time-lagged correlation analysis (Jourdain *et al*., 2013). Interestingly, models with strong ENSO-monsoon relationship also show strong negative correlation between Nino 3.4 and NP1 SST anomalies, which is closer to observations. The models with poor ENSO-monsoon relationship (CC close to zero) do not show clear relationship between SST anomalies over Nino 3.4 and NP1. We conclude here that SST over NP1 modulates the ENSO-monsoon relationship. Thus, a realistic simulation of SST over NP1 relating to Nino 3.4 anomalies is necessary to capture the observed strength of ENSO-monsoon relationship.

4. Conclusions

This study illustrates the role of east-west variation of SST anomaly over NPAC in the changes in circulation and convection during northern summer season. It was seen that zonally symmetric SST warming shifts the 200 hPa jet towards north by about 15 degrees over a wide longitude belt. On the other hand, zonally asymmetric anomalies with warming along western NPAC and cooling over the central parts induce phase shift in Rossby waves such that the meridional winds over Indian region become anomalously northerly. Zonally symmetric SST anomaly at the equatorial Pacific Ocean (ENSO modes) shows largest impact on circulation in the Tropics. These changes in circulation and temperature modulate the VMS of the atmosphere. The changes in VMS were found to have large impact on the intensity of monsoon rainfall over India. The zonally asymmetric SST anomaly away from the equator, through shift of phase of the Rossby waves, impacts ISM more compared to zonally symmetric off-equatorial or equatorial anomalies. The northeast *vs* southwest asymmetry in precipitation anomaly over Indian region experienced in several years can be explained through this asymmetric SST mode of NPAC. The precipitation changes were spatially coherent for zonally symmetric equatorial and off-equatorial SST modes.

It is also found that this relationship between SST of NPAC and Indian monsoon precipitation can be used, in conjunction with the SST of equatorial Pacific and Indian Oceans, to construct an index that can explain about 82% of the interannual variability of precipitation in India in June-July during the satellite era, when accurate measurement of SST around the globe is available. When SSTs of NPAC are not included to construct the index, the variance explained drops down to about 50%.

Finally, using simulations of 36 CMIP5 models with historical scenario, we show the robustness of our above-mentioned results. We show that those models capture the out-of-phase relationship in SST anomaly between Nino 3.4 and NP1 (as in observations) also realistically simulates anomaly of rainfall over Indian region during both El Nino and La Nina years. This result shows the importance of simulating the realistic see-say in SST anomalies between NP1 and Nino 3.4 in order to get the interannual variation of Indian summer monsoon. The teleconnection mechanism proposed in this study, thus, can be used to diagnose general circulation models those in general do not show a realistic relationship between SST and ISM.

Acknowledgements

This work was partially supported by Department of Science and Technology, Govt of India; and Ministry of Earth Sciences, Govt of India. The SST data was obtained from NOAA/NCDC website. The gridded rainfall data can be obtained upon request from India Meteorological Department and is widely used in different studies. All-India homogeneous regions averaged rainfall data can be obtained from the website of the Indian Institute of Tropical Meteorology. The NOAA/OAR/ESRL PSD, Boulder, Colorado, USA provided interpolated OLR data, from their Web site at http://www.esrl.noaa.gov/psd/. Data of other atmospheric variables used in this study was obtained from ECMWF web portal (ERA-Interim).

The contents and views expressed in this research paper are the views of the authors and do not necessarily reflect the views of the organizations they belong to.

References

Ambrizzi, T. and Hoskins, B. J., 1997, "Stationary rossby-wave propagation in a baroclinic atmosphere", *Quarterly Journal of the Royal Meteorological Society*, **123**, 919-928, doi:10.1002/qj.49712354007.

Ashok, K., Behera, S., Rao, S., Weng, H. and Yamagata, T., 2007, "El Niño Modoki and its possible teleconnection", *Journal of Geophysical Research: Oceans, (1978-2012)*, **112**, C11008, https://dx.doi.org/10.1029/2006jc003798.

Baohua, R. and Ronghui, H., 2002, "10-25-day intraseasonal variations of convection and circulation associated with thermal state of the western Pacific warm pool during boreal summer", *Advances in Atmospheric Sciences*, **19**, 2, 321-336. https://dx.doi.org/10.1007/s00376-002-0025-9.

Bhatla, R., Gyawali, B., Mall, R. K. and Raju, P. V. S., 2013, "Study of possible linkage of PDO with Indian summer monsoon in relation to QBO", *Vayumandal*, **39**, 1-2, 40-45.

Boschat, G., Terray, P. and Masson, S., 2010, "Interannual relationships between Indian Summer Monsoon and Indo-Pacific coupled modes of variability during recent decades", *Climate Dynamics*, **37**, 1019-1043, doi:10.1007/s00382-010-0887-y.

Chakraborty, A. and Agrawal, S., 2017, "Role of west Asian surface pressure in summer monsoon onset over central India", *Environmental Research Letters*, **12**, 7, 074002, https://dx.doi.org/10.1088/1748-9326/aa76ca.

Chakraborty, A., 2018, "Preceding winter La Niña reduces Indian summer monsoon rainfall", *Environmental Research Letters*, **13**, 5, 054030, https://dx.doi.org/10.1088/1748-9326/aabdd5.

Chakraborty, A., Nanjundiah, R. S. and Srinivasan, J., 2006, "Theoretical aspects of the onset of Indian summer monsoon from perturbed orography simulations in a GCM", *Ann. Geophys.*, **24**, 2075-2089, doi:10.5194/angeo-24-2075-2006.

Chakraborty, A., Nanjundiah, R. S. and Srinivasan, J., 2014, "Local and remote impacts of direct aerosol forcing on Asian monsoon", *International Journal of Climatology*, **34**, 2108-2121, doi:10.1002/joc.3826.

Chang, C., Zhang, Y. and Li, T., 2000, "Interannual and Interdecadal Variations of the East Asian Summer Monsoon and Tropical Pacific SSTs. Part I: Roles of the Subtropical Ridge", *Journal of Climate*, **13**, 24, 4310-4325, https://dx.doi.org/10.1175/1520-0442(2000)013<4310:iaivot>2.0.co;2.

Chattopadhyay, J. and Bhatla, R., 1993, "Sea surface temperature anomaly over equatorial Pacific Ocean as a predictor of Indian summer monsoon rainfall", *Vayu Mandal*, **23**, 4-6.

Chattopadhyay, J. and Bhatla, R., 2002, "Possible influence of QBO on teleconnections relating Indian summer monsoon rainfall and sea surface temperature anomalies across equatorial Pacific", *International Journal of Climatology*, **22**, 1, 121-127.

Chen, T. and Chen, J., 1993, "The 10-20-Day Mode of the 1979 Indian Monsoon: Its Relation with the Time Variation of Monsoon Rainfall", *Monthly Weather Review*, **121**, 9, 2465-2482, https://dx.doi.org/10.1175/1520-0493(1993)121<2465:tdmoti>2.0.co;2.

Dee, D. P., Uppala, S. M., Simmons, A. J., Berrisford, P., Poli, P., Kobayashi, S., Andrae, U., Balmaseda, M. A., Balsamo, G., Bauer, P., Bechtold, P., Beljaars, A. C. M., Van de Berg, L., Bidlot, J., Bormann, N., Delsol, C., Dragani, R., Fuentes, M., Geer, A. J., Haimberger, L., Healy, S. B., Hersbach, H., Hólm, E. V., Isaksen, L., Kallberg, P., Köhler, M., Matricardi, M., McNally, A. P., Monge-Sanz, B. M., Morcrette, J. J., Park, B. K., Peubey, C., De Rosnay, P., Tavolato, C., Thépaut, J. N. and Vitart, F., 2011, "The ERA-Interim reanalysis: configuration and performance of the data assimilation system", *Quarterly Journal of the Royal Meteorological Society*, **137**, 656, 553-597, doi:10.1002/qj.828.

Ding, Q. and Wang, B., 2005, "Circumglobal teleconnection in the Northern Hemisphere summer", *Journal of Climate*, **18**, 3483-3505, doi:10.1175/JCLI3473.1.

Ding, Q. and Wang, B., 2007, "Intraseasonal Teleconnection between the Summer Eurasian Wave Train and the Indian Monsoon", *Journal of Climate*, **20**, 3751-3767, doi:10.1175/JCLI4221.1.

Hoskins, B. J. and Ambrizzi, T., 1993, "Rossby wave propagation on a realistic longitudinally varying flow", *J. Atmos. Sci.*, **50**, 1661-1671, doi:10.1175/1520-0469(1993)050<1661:R WPOA R>2.0.CO;2.

Hunt, B. G., 2014, "The influence of stochasticism on Indian summer monsoon rainfall and its impact on prediction", *Climate Dynamics*, **42**, 9-10, 2271-2285, doi:10.1007/s00382-014-2119-3.

Jayasankar, C. B., Surendran, S. and Rajendran, K., 2015, "Robust signals of future projections of Indian summer monsoon rainfall by IPCC AR5 climate models: Role of seasonal cycle and interannual variability", *Geophysical Research Letters*, **42**, 3513-3520, doi:10.1002/2015GL063659.

Jourdain, N. C., Sen Gupta, A., Taschetto, A. S., Ummenhofer, C. C., Moise, A. F. and Ashok, K., 2013, "The Indo-Australian monsoon and its relationship to ENSO and IOD in reanalysis data and the CMIP3/CMIP5 simulations", *Climate Dynamics*, **41**, 3073-3102, doi:10.1007/s00382-013-1676-1.

Karmakar, N., Chakraborty, A. and Nanjundiah, R., 2017, "Space-Time Evolution of the Low- and High-Frequency Intraseasonal Modes of the Indian Summer Monsoon", *Monthly Weather Review*, **145**, 2, 413-435, https://dx.doi.org/10.1175/mwr-d-16-0075.1.

Kaspi, Y. and Schneider, T., 2011, "Winter cold of eastern continental boundaries induced by warm ocean waters", *Nature*, **471**, 621-624, doi:10.1038/nature09924.

Krishnamurthy, L. and Krishnamurthy, V., 2014, "Influence of PDO on South Asian summer monsoon and monsoon-ENSO relation", *Climate Dynamics*, **42**, 9-10, 2397-2410, https://dx.doi.org/10.1007/s00382-013-1856-z.

Krishnamurthy, V. and Goswami, B. N., 2000, "Indian monsoon-ENSO relationship on interdecadal timescale", *Journal of Climate*, **13**, 579-595, doi:10.1175/1520-0442(2000)013<0579:IMEROI>2.0.CO;2.

Krishnamurti, T. and Ardanuy, P., 1980, "The 10 to 20-day westward propagating mode and Breaks in the Monsoons", *Tellus A*, **32**, 1, 15-26, https://dx.doi.org/10.3402/tellusa.v32i1.10476.

Krishnan, R. and Sugi, M., 2003, "Pacific decadal oscillation and variability of the Indian summer monsoon rainfall", *Climate Dynamics*, **21**, 3-4, 233-242, https://dx.doi.org/10.1007/s00382-003-0330-8.

Kumar, K. K., Rajagopalan, B. and Cane, M. A., 1999, "On the weakening relationship between the Indian Monsoon and ENSO", *Science*, **284**, 2156-2159, doi:10.1126/science.284.5423.2156.

Lau, N. and Nath, M., 2000, "Impact of ENSO on the Variability of the Asian-Australian Monsoons as Simulated in GCM Experiments", *Journal of Climate*, **13**, 24, 4287-4309, https://dx.doi.org/10.1175/1520-0442(2000)013<4287:ioeotv>2.0.co;2.

Liebmann, B. and Smith, C. A., 1996, "Description of a complete (interpolated) outgoing longwave radiation dataset", *Bulletin of the American Meteorological Society*, **77**, 6, 1275-1277.

Lu, J., Chen, G. and Frierson, D., 2008, "Response of the Zonal Mean Atmospheric Circulation to El Niño versus Global Warming", *Journal of Climate*, **21**, 22, 5835-5851, https://dx.doi.org/10.1175/2008jcli2200.1.

Mantua, N. J. and Hare, S. R., 2002, "The Pacific Decadal Oscillation", *Journal of Oceanography*, **58**, 35-44, doi:10.1023/A:1015820616384.

Mantua, N., Hare, S., Zhang, Y., Wallace, J. and Francis, R., 1997, "A Pacific Interdecadal Climate Oscillation with Impacts on Salmon Production", *Bulletin of the American Meteorological Society*, **78**, 6, 1069-1079, https://dx.doi.org/10.1175/1520-0477(1997)078<1069:apicow>2.0.co;2.

Meehl, G. A. and Arblaster, J. M., 2011, "Decadal Variability of Asian-Australian Monsoon-ENSO-TBO Relationships", *Journal of Climate*, **24**, 4925-4940, doi:10.1175/2011JCLI4015.1.

Mooley, D. A. and Parthasarathy, B., 1984, "Fluctuations in All-India summer monsoon rainfall during 1871-1978", *Climatic Change*, **6**, 287-301, doi:10.1007/BF00142477.

Nanjundiah, R. S. and Srinivasan, J., 1999, "Anomalies of precipitable water vapour and vertical stability during El Nino", *Geophysical Research Letters*, **26**, 95-98, doi:10.1029/1998GL900254.

Neelin, J. D. and Held, I. M., 1987, "Modeling tropical convergence based on the moist static energy budget", *Mon. Wea. Rev*., **115**, 3-12, doi:10.1175/1520-493(1987)115<0003:MTCBOT>2.0.CO;2.

Nidheesh, A., Lengaigne, M., Vialard, J., Izumo, T., Unnikrishnan, A. and Cassou, C., 2017, "Influence of ENSO on the Pacific decadal oscillation in CMIP models", *Climate Dynamics*, **49**, 9-10, 3309-3326.

Peings, Y., Douville, H. and Terray, P., 2009, "Extended winter Pacific North America oscillation as a precursor of the Indian summer monsoon rainfall", *Geophysical Research Letters*, **36**, 11, L11710, https://dx.doi.org/10.1029/2009gl038453.

Rajeevan, M., Bhate, J., Kale, J. D. and Lal, B., 2006, "High resolution daily gridded rainfall data for the Indian region: Analysis of break and active", *Current Science*, **91**, 3, 296-306.

Reynolds, R., Rayner, N., Smith, T., Stokes, D. and Wang, W., 2002, "An Improved In Situ and Satellite SST Analysis for Climate", *Journal of Climate*, **15**, 13, 1609-1625, https://dx.doi.org/10.1175/1520-0442(2002)015<1609:aiisas>2.0.co;2.

Ronghui, H. and Yifang, W., 1989, "The influence of ENSO on the summer climate change in China and its mechanism", *Advances in Atmospheric Sciences*, **6**, 1, 21-32, https://dx.doi.org/10.1007/ bf02656915.

Saji, N. H., Goswami, B. N. and Vinayachandran, P. N., 1999, "A dipole mode in the tropical Indian Ocean", *Nature*, **401**, 360-363, doi:10.1038/43854.

Seager, R., Harnik, N., Kushnir, Y., Robinson, W. and Miller, J., 2003, "Mechanisms of Hemispherically Symmetric Climate Variability", *Journal of Climate*, **16**, 18, 2960-2978, https://dx.doi.org/10.1175/1520-0442(2003)016<2960:mohscv>2.0.co;2.

Shaman, J. and Tziperman, E., 2007, "Summertime ENSO-North African-Asian Jet teleconnection and implications for the Indian monsoons", *Geo. Res. Lett.*, **34**, 11, L11702-L11707, doi:10.1029/2006GL029143.

Shen, S. and Lau, K., 1995, "Biennial Oscillation Associated with the East Asian Summer Monsoon and Tropical Sea Surface Temperatures", *Journal of the Meteorological Society of Japan*, *Ser. II*, **73**, 1, 105-124, https://dx.doi.org/10.2151/jmsj1965.73.1_105.

Shukla, J. and Mooley, D., 1987, "Empirical Prediction of the Summer Monsoon Rainfall over India", *Monthly Weather Review*, **115**, 3, 695-704, https://dx.doi.org/10.1175/1520-0493(1987)115<0695:epotsm>2.0.co;2.

Shukla, J. and Paolino, D., 1983, "The Southern Oscillation and Long-Range Forecasting of the Summer Monsoon Rainfall over India", *Monthly Weather Review*, **111**, 9, 1830-1837, https://dx.doi.org/10.1175/1520-0493(1983)111<1830:tsoalr>2.0.co;2.

Sikka, D., 1980, "Some aspects of the large scale fluctuations of summer monsoon rainfall over India in relation to fluctuations in the planetary and regional scale circulation parameters", *Proceedings of the Indian Academy of Sciences - Earth and Planetary Sciences*, **89**, 2, 179-195, https://dx.doi.org/10.1007/bf02913749.

Sperber, K. R., Annamalai, H., Kang, I. S., Kitoh, A., Moise, A., Turner, A., Wang, B. and Zhou, T., 2013, "The Asian summer monsoon: An intercomparison of CMIP5 *vs*. CMIP3 simulations of the late 20th century", *Climate Dynamics*, **41**, 2711-2744, doi:10.1007/s00382-012-1607-6.

Srinivasan, J. and Smith, G. L., 1996, "The role of heat fluxes and moist static energy in tropical convergence zones", *Mon. Wea. Rev*., **124**, 2089-2099, doi:10.1175/1520-0493(1996)124<2089:TROHFA>2.0.CO;2.

Srivastava, G., Chakraborty, A. and Nanjundiah, R., 2019, "Multidecadal see-saw of the impact of ENSO on Indian and West African summer monsoon rainfall", *Climate Dynamics*, **52**, 11, 6633-6649, https://dx.doi.org/10.1007/s00382-018-4535-2.

Terray, P., Delécluse, P., Labattu, S. and Terray, L., 2003, "Sea surface temperature associations with the late Indian summer monsoon", *Climate Dynamics*, **21**, 7-8, 593-618.

Torrence, C. and Webster, P. J., 1999, "Interdecadal changes in the ENSO-monsoon system", *Journal of Climate*, **12**, 2679-2690, doi:10.1175/1520-0442(1999)012<2679:ICITEM>2.0.CO;2.

Vimont, D., Battisti, D. and Hirst, A., 2001, "Footprinting: A seasonal connection between the tropics and mid-latitudes", *Geophysical Research Letters*, **28**, 20, 3923-3926, https://dx.doi.org/10.1029/2001gl013435.

Vimont, D., Wallace, J. and Battisti, D., 2003, "The Seasonal Footprinting Mechanism in the Pacific: Implications for ENSO", *Journal of Climate*, **16**, 16, 2668-2675, https://dx.doi.org/10.1175/1520-0442(2003)016<2668:tsfmit>2.0.co;2.

Wang, B., Wu, R. and Fu, X., 2000, "Pacific-East Asian Teleconnection: How Does ENSO Affect East Asian Climate?", *Journal of Climate*, **13**, 9, 1517-1536, https://dx.doi.org/10.1175/1520-0442(2000)013<1517:peathd>2.0.co;2.

Wang, S., Huang, J., He, Y. and Guan, Y., 2014, "Combined effects of the Pacific Decadal Oscillation and El Niño-Southern Oscillation on Global Land Dry-Wet Changes", *Scientific Reports*, **4**, 1, 6651, https://dx.doi.org/10.1038/srep06651.

Zang, Y., Wallace, J. M. and Battisti, D. S., 1997, "ENSO-like interdecadal variability: 1900-1993", *Journal of Climate*, **10**, 5, 1004-1020.